Journal of Organometallic Chemistry 694 (2009) 3050–3057

Contents lists available at ScienceDirect

Journal of Organometallic Chemistry

journal homepage: www.elsevier.com/locate/jorganchem

Highly efficient phosphorescent iridium (III) diazine complexes for OLEDs: Different photophysical property between iridium (III) pyrazine complex and iridium (III) pyrimidine complex

Guoping Ge [a], Jing He [b], Haiqing Guo [a,*], Fuzhi Wang [c], Dechun Zou [c,*]

[a] Beijing National Laboratory for Molecular Sciences, State Key Laboratory of Rare Earth Materials Chemistry and Applications, College of Chemistry and Molecular Engineering, Peking University, 5 Yiheyuan Road, Haidian District, Beijing 100871, China
[b] College of Materials Science and Technology, Beijing Forestry University, Beijing 100083, China
[c] Key Laboratory of Polymer Chemistry and Physics of Education Ministry, Department of Polymer Science and Engineering, College of Chemistry and Molecular Engineering, Peking University, 5 Yiheyuan Road, Haidian District, Beijing 100871, China

ARTICLE INFO

Article history:
Received 7 April 2009
Received in revised form 25 May 2009
Accepted 26 May 2009
Available online 6 June 2009

Keywords:
Phosphorescence
Iridium diazine complex
^{3}MLCT
OLED

ABSTRACT

The synthesis and luminescence of four new iridium (III) diazine complexes (**1–4**) were investigated. HOMO and LUMO energy levels of the complexes were estimated according to the electrochemical performance and the UV–Vis absorption spectra, showing the pyrimidine complexes have a larger increase for the LUMO than the HOMO orbital in comparison with the pyrazine complexes. Several high-efficiency yellow and green OLEDs based on phosphorescent iridium (III) diazine complexes were obtained. The devices emitting yellow light based on **1** with turn-on voltage of 4.1 V exhibited an external quantum efficiency of 13.2% (power efficiency 20.3 lm/W), a maximum current efficiency of 37.3 cd/A. The electroluminescent performance for the green iridium pyrimidine complex of **3** is comparable to that of the iridium pyridine complex $(PPY)_2Ir(acac)$ (PPY = 2-phenylpyridine), which is among the best reported.
© 2009 Elsevier B.V. All rights reserved.

1. Introduction

Organic light-emitting diodes (OLEDs) based on phosphorescent materials have significantly improved electroluminescence (EL) performance because both singlet and triplet excitons can be harvested for light emission. Theoretically, the internal quantum efficiency of phosphorescent emitters can approach 100% [1,2]. Among the research of phosphorescent materials, rationally tuning the emission wavelength of heavy-metal phosphorescent emitters over the entire visible range has emerged as an important ongoing research task [3]. Iridium (III) complexes are highly tunable in the emission color [4]. Modifying the skeletal arrangement as well as the substituent groups of the cyclometalating ligand (C^N), where C^N is usually a C-2 metalated 2-phenylpyridine (PPY) ligand or analogs, afford significant tuning of phosphorescence [4–7]. Using appropriate ancillary ligands also cause shifting of the emission from the red to the blue region [8–10]. Despite OLEDs with iridium (III) diazine complexes as phosphor have high-efficiency and long luminance half-life [3,11–16], investigations focused on using diazine as a ligand for iridium complex for OLEDs are still insufficient.

We got succeeded in preparation of several efficient red and yellow OLEDs based on the phosphorescent iridium (III) pyrazine complexes [15–18] and reported a polymer-based blue electrophosphorescent light-emitting diodes based on an iridium (III) pyrimidine complex recently [19]. The results inspired us to initiate a systematic study on the different photophysical property between iridium (III) pyrazine complex and iridium (III) pyrimidine complex. In this paper, we report the synthesis and characterization of four new iridium (III) diazine complexes. Among of them, two are iridium (III) pyrazine complexes, the other two are iridium (III) pyrimidine complexes. Their structure-photophysical property relationships were investigated. Several high-efficiency yellow and green OLEDs based on phosphorescent iridium (III) diazine complexes were obtained.

2. Experimental

2.1. Measurement

^{1}H NMR spectra were measured on a Mercury Plus 300 spectrometer in $CDCl_3$ using tetramethylsilane as an internal reference. Elemental analyses were performed on an Elementary Vario EL instrument. Mass spectra were measured on a Bruker BIFLEX III mass spectrophotometer or Bruker Apex IV FTMS. UV–Vis absorption spectra were recorded using a Shimadzu UV-2550 spectrophotometer. Emission spectra were measured on a Hitachi F-4500 fluorescence spectrophotometer.

* Corresponding authors. Fax: +86 10 62755702 (H. Guo).
E-mail address: guohq@pku.edu.cn (H. Guo).

0022-328X/$ - see front matter © 2009 Elsevier B.V. All rights reserved.
doi:10.1016/j.jorganchem.2009.05.037

Cyclic voltammetry was performed with a computer-controlled EG&G potentiostat/galvanostat model 283 in a one-compartment electrolysis cell consisting of a platinum bottom working electrode, a platinum wire counter electrode, and an Ag/AgCl reference electrode. Cyclic voltammograms were monitored at scan rate of 50 mV s^{-1} and recorded in HPLC-grade dichloromethane. The concentration of the complex was maintained at 1.0 mM and each solution contained 0.1 M of tetrabutylammonium hexafluorophosphate (TBAP) as the electrolyte. The highest occupied molecular orbital (HOMO) and the lowest unoccupied molecular orbital (LUMO) energy level were calculated by assuming the energy level of ferrocene/ferrocenium to be −4.8 eV.

2.2. Synthesis

2.2.1. General procedure for the synthesis of diazine ligands

Diazine ligands (abbreviated with the general formula **da**) 2-phenylpyrazine (**PPZ**), 2-(2,4-difluorophenyl)-pyrazine (**DFPPZ**), 2-methyl-3-phenylpyrazine (**MPPZ**), 2-(2,4-difluorophenyl)-3-methylpyrazine (**DFMPPZ**), 2-phenylpyrimidine (**PPM**) and 2-(2,4-difluorophenyl)-pyrimidine (**DFPPM**) were obtained from the reaction of chlorodiazines and the corresponding arylboronic acids by a similar procedure [20], so that a detailed description is provided only for **MPPZ**. 4-Phenylpyrimidine (**4-PPM**) and 4-(2,4-difluorophenyl)-pyrimidine (**4-DFPPM**) were prepared according to the similar procedure previously reported [21].

*2.2.1.1. Synthesis of **MPPZ**.* 3.23 g of 2-chloro-3-methylpyrazine (1 equiv.; 25 mmol), 3.66 g of phenylboronic acid (1.2 equiv.; 30 mmol) and 0.66 g of triphenylphosphine (0.1 equiv.; 2.5 mmol) were dissolved in 1,2-dimethoxyethane (25 mL). 34 mL of a 2 M K_2CO_3 (2.7 equiv.; 67.5 mmol) aqueous solution were added and the mixture was purged with nitrogen. Palladium acetate (0.14 g; 0.025 equiv.) was added and the mixture was refluxed for 18 h. The two phases were then separated and the aqueous phase was extracted with ethyl acetate (4 × 60 mL). The combined organic phases were washed with water (80 mL) and brine (80 mL) and were dried over $MgSO_4$. After evaporation of the solvent, a yellow powder was obtained. The crude product was chromatographed using a dichloromethane:acetone = 20:1 column to yield 65% of the pure **MPPZ** as pale yellow crystals after solvent evaporation and drying. Anal. Calc. for $C_{11}H_{10}N_2$: C, 77.62; H, 5.92; N, 16.46. Found: C, 77.41; H, 6.01; N, 16.41%. ^{1}H NMR ($CDCl_3$, 300 MHz) δ: 8.51(d, 1H), 8.46(d, 1H), 7.62–7.52(m, 2H), 7.53-7.48(m, 3H), 2.65 (s, 3H). EI-MS: Calc. for $C_{11}H_{10}N_2$ 170; Found 170.

*2.2.1.2. **PPZ**.* Yellow powders. Yield: 57%. Anal. Calc. for $C_{10}H_8N_2$: C, 76.90; H, 5.16; N, 17.94. Found: C,76.87; H, 5.04; N, 18.20%. ^{1}H NMR ($CDCl_3$, 300 MHz) δ: 9.04(s, 1H), 8.64(d, 1H), 8.51(d, 1H), 8.03(m, 2H), 7.50(m, 3H). EI-MS: Calc. for $C_{10}H_8N_2$ 156; Found 156.

*2.2.1.3. **DFPPZ**.* Pale yellow powders. Yield: 45%. Anal. Calc. for $C_{10}H_6F_2N_2$: C, 62.50; H, 3.15; N, 14.58. Found: C, 62.66; H, 3.34; N, 14.22%. ^{1}H NMR ($CDCl_3$, 300 MHz) δ: 9.08(s, 1H), 8.69(d, 1H), 8.54(d, 1H), 8.04(m, 1H), 7.01(m, 2H). EI-MS: Calc. for $C_{10}H_6F_2N_2$ 192; Found 192.

*2.2.1.4. **DFMPPZ**.* Yellow powders. Yield: 63%. Anal. Calc. for $C_{11}H_8F_2N_2$: C, 64.08; H, 3.91; N, 13.59. Found: C, 63.82; H, 3.82; N, 13.24%. ^{1}H NMR ($CDCl_3$, 300 MHz) δ: 8.51(s, 2H), 7.48(m, 1H), 7.08–6.93(m, 2H), 2.52(s, 3H). EI-MS: Calc. for $C_{11}H_8F_2N_2$ 206; Found 206.

*2.2.1.5. **PPM**.* Pale yellow crystals. Yield: 61%. Anal. Calc. for $C_{10}H_8N_2$: C, 76.90; H, 5.16; N, 17.94. Found: C,76.80; H, 5.25; N, 17.98%. ^{1}H NMR ($CDCl_3$, 300 MHz) δ: 8.81(d, 2H), 8.46(m, 2H), 7.51(m, 3H), 7.18(m,1H). EI-MS: Calc. for $C_{10}H_8N_2$ 156; Found 156.

*2.2.1.6. **DFPPM**.* Yellow powders. Yield: 79%. Anal. Calc. for $C_{10}H_6F_2N_2$: C, 62.50; H, 3.15; N, 14.58. Found: C, 62.68; H, 2.97; N, 14.36%. ^{1}H NMR ($CDCl_3$, 300 MHz) δ: 8.86(d, 2H), 8.13(m, 1H), 7.31(m, 1H), 6.98(m, 2H). EI-MS: Calc. for $C_{10}H_6F_2N_2$ 192; Found 192.

*2.2.1.7. **4-PPM**.* Pale yellow powders. Yield: 51%. Anal. Calc. for $C_{10}H_8N_2$: C, 76.90; H, 5.16; N, 17.94. Found: C,77.03; H, 5.03; N, 18.27%. ^{1}H NMR ($CDCl_3$, 300 MHz) δ: 9.29(s, 1H), 8.79(d, 1H), 8.11(m, 2H), 7.74(m, 1H), 7.54(m, 3H). EI-MS: Calc. for $C_{10}H_8N_2$ 156; Found 156.

*2.2.1.8. **4-DFPPM**.* Pale yellow powders. Yield: 33%. Anal. Calc. for $C_{10}H_6F_2N_2$: C, 62.50; H, 3.15; N, 14.58. Found: C, 62.75; H, 2.94; N, 14.53%. ^{1}H NMR ($CDCl_3$, 300 MHz) δ: 9.30(s, 1H), 8.79(d, 1H), 8.27(m, 1H), 7.84(d, 1H), 7.02(m, 2H). EI-MS: Calc. for $C_{10}H_6F_2N_2$ 192; Found 192.

2.2.2. General procedure for the synthesis of the iridium complexes

All synthetic procedures involving $IrCl_3{\cdot}3H_2O$ and other Ir(III) species were carried out in inert gas atmosphere despite the air stability of the compounds, the main concern being the oxidative stability of intermediate complexes at the high temperatures used in the reactions [6]. Cyclometalated Ir(III) μ-chloro-bridged dimers of general formula (**da**)$_2$Ir(μ-Cl)$_2$Ir(**da**)$_2$, where **da** represents the cyclometalated diazine, were synthesized by the same method reported by Nonoyama [22]. The crude products of these dimers were used for subsequent preparation of (**da**)$_2$Ir(acac). Only the syntheses of (**MPPZ**)$_2$Ir(acac) (**4**) will be described in detail.

*2.2.2.1. Synthesis of (**MPPZ**)$_2$Ir (acac).* Cyclometalated Ir(III)-chloro-bridged dimers [(**MPPZ**)$_2$IrCl]$_2$ were synthesized according to the Nonoyama route, by refluxing $IrCl_3{\cdot}3H_2O$ with 2.2 equiv. of **MPPZ** in a 3:1 mixture of 2-ethoxyethanol and water [22]. The reaction mixture was refluxed under nitrogen atmosphere for 24 h. After cooling to room temperature, a precipitate was collected by suction and washed with ethanol, acetone, and then dried in vacuum to give crude [(**MPPZ**)$_2$IrCl]$_2$ as an orange powder. The crude [(**MPPZ**)$_2$IrCl]$_2$ (0.4 mmol), 1.2 mmol of acetyl acetone and 0.33 g of sodium carbonate were refluxed under nitrogen atmosphere in 20 mL of 2-ethoxyethanol for 15 h. After the reaction mixture was cooled to room temperature, the precipitate was filtered off and washed with water, ethanol, and ether to afford orange powdery (**MPPZ**)$_2$Ir(acac) (**1**) in 61% yield. Anal. Calc. for $C_{27}H_{25}IrN_4O_2$: C, 51.50; H, 4.00; N, 8.90. Found: C, 51.27; H, 4.17; N, 8.73%. ^{1}H NMR ($CDCl_3$, 300 MHz) δ: 8.45(d, 2H), 8.22(d, 2H), 7.92(d, 2H), 6.91(t, 2H), 6.74 (t, 2H), 6.25(d, 2H), 5.23(s, 1H), 3.10(s, 6H), 1.80(s, 6H). EI-MS: Calc. for $C_{27}H_{25}IrN_4O_2$ 630; Found 630.

*2.2.2.2. (**DFMPPZ**)$_2$Ir(acac) (**2**), Iridium (III) bis(2-(2,4-difluorophenyl)-3-methylpyrazine-N,C$^{2'}$) (acetylacetonate).* Yellow powders. Yield: 67%. Anal. Calc. for $C_{27}H_{21}F_4IrN_4O_2$: C, 46.22; H, 3.02; N, 7.98. Found: C, 45.95; H, 3.05; N, 8.04%. ^{1}HNMR ($CDCl_3$, 300 MHz) δ: 8.34(d, 2H), 8.24(d, 2H), 6.42(m, 2H), 5.60(m, 2H), 5.26(s, 1H), 2.91(s, 3H), 2.85(s, 3H), 1.81(s, 6H). EI-MS: Calc. for $C_{27}H_{21}F_4IrN_4O_2$ 702; Found 702.

*2.2.2.3. (**PPM**)$_2$Ir(acac) (**3**), Iridium (III) bis(2-phenylpyrimidine-N,C$^{2'}$) (acetylacetonate).* Yellow powders. Yield: 20%. Anal. Calc. for $C_{25}H_{21}IrN_4O_2$: C, 49.91; H, 3.52; N, 9.31. Found: C, 49.58; H, 3.69; N, 8.97%. ^{1}HNMR ($CDCl_3$, 300 MHz) δ: 8.78(m, 2H), 8.66(m, 2H), 7.96(m, 2H), 7.14(t, 2H), 6.88(m, 2H), 6.81(m, 2H), 6.33(d, 2H),

5.23(s, 1H), 1.80(s, 6H). EI-MS: Calc. for $C_{25}H_{21}IrN_4O_2$ 602; Found 602.

*2.2.2.4. (**DFPPM**)$_2$Ir(acac) (**4**), Iridium (III) bis(2-(2,4-difluorophenyl)-pyrimidine-N,C$^{2'}$) (acetylacetonate).* Yellow powders. Yield: 56%. Anal. Calc. for $C_{25}H_{17}F_4IrN_4O_2$: C, 44.57; H, 2.54; N, 8.32. Found: C, 44.28; H, 2.73; N, 8.11%. ^{1}HNMR ($CDCl_3$, 300 MHz) δ: 8.90(m, 2H), 8.59(m, 2H), 7.10(t, 2H), 6.43(m, 2H), 5.75(m, 2H), 5.24(s, 1H), 1.83(s, 6H). ESI-MS: Calc. for $C_{25}H_{18}F_4IrN_4O_2$ 675.09896; Found m/z 675.10118 [M+H$^+$].

2.3. OLEDs fabrication and measurements

The device was fabricated with a standard vacuum–vapor deposition process. The emitting area was 2 × 2 mm and all OLEDs were formed on the same glass substrate. 4,4-bis[N-(1-naphthyl)-N-phenyl-amino]biphenyl (NPB) – the hole transporter – was first deposited on the indium tin oxide (ITO)-coated glass. The NPB layer was followed by a layer of 4,4′-*N*,*N*′-dicarbazole-biphenyl (CBP) doped with Iridium complexes. Layers of TPBI – to serve as the hole-blocker and electron-transporter; tri-(8-hydroxyquinoline) aluminum(III) (Alq_3) – as the electron-transporter; and Mg:Ag/Ag – as the cathode, were successively deposited. The EL spectra were measured with a spectrofluorometer FP-6200 (JASCO), a source-measure unit R6145(Advantest), multimeter 2000(Keithley) and luminance was directly detected by using a multifunctional optical meter 1835-C(Newport). All the measurements were automatically controlled by a computer system, and only about 400 ms are needed to get one *L–J–V* curve by using our measuring system. The quantum efficiency was calculated by using the luminescence, emission spectra and current density data.

3. Results and discussion

3.1. Synthesis of the materials

Standard procedure was followed to synthesize diazine ligands from chlorodiazines and appropriate arylboronic acids, as illustrated in (a) of Scheme 1, using **MPPZ** as the representative example. The syntheses of the bis-cyclometalated iridium complexes of diazines are shown in Scheme 1, using (**MPPZ**)$_2$Ir (acac) as the representative example: (b) reaction of $IrCl_3{\cdot}3H_2O$ with diazine ligand to form a chloride-bridged dimer, (**da**)$_2$Ir(μ-Cl)$_2$Ir(**da**)$_2$ (**da** = cyclometalated diazine); (c) replacement of bridging chlorides with bidentate β-diketonate ligands to give the desired products, (**da**)$_2$Ir(acac) (acac = acetylacetonate); Chart 1 shows the complexes (**da**)$_2$Ir(acac) synthesized in this study.

In addition, reactivity of diazine ligands with iridium ion in synthesis of iridium complex was investigated. **MPPZ** and **DFMPPZ** can react with Ir(III) successfully to form corresponding iridium complex, but **PPZ** and **DFPPZ** cannot. These results suggest that steric influence of methyl group in **MPPZ** and **DFMPPZ** may play an important role in the cyclometalating procedure. Ir(III) can selectively attack on the 1-position nitrogen atom in the presence of methyl group, whereas 4-position nitrogen atom in **PPZ** and **DFPPZ** may also react with Ir(III) that cause many by-products (Fig. 1).

Furthermore, it was also found that symmetry of the ligand structure may also play an important role. We got succeeded in preparation of the iridium complexes with **PPM** or **DFPPM** as ligand that has two symmetrical nitrogen atoms beside the phenyl ring. However, we got failed in preparation of the iridium complexes with **4-PPM** or **4-DFPPM** as ligand at the same condition.

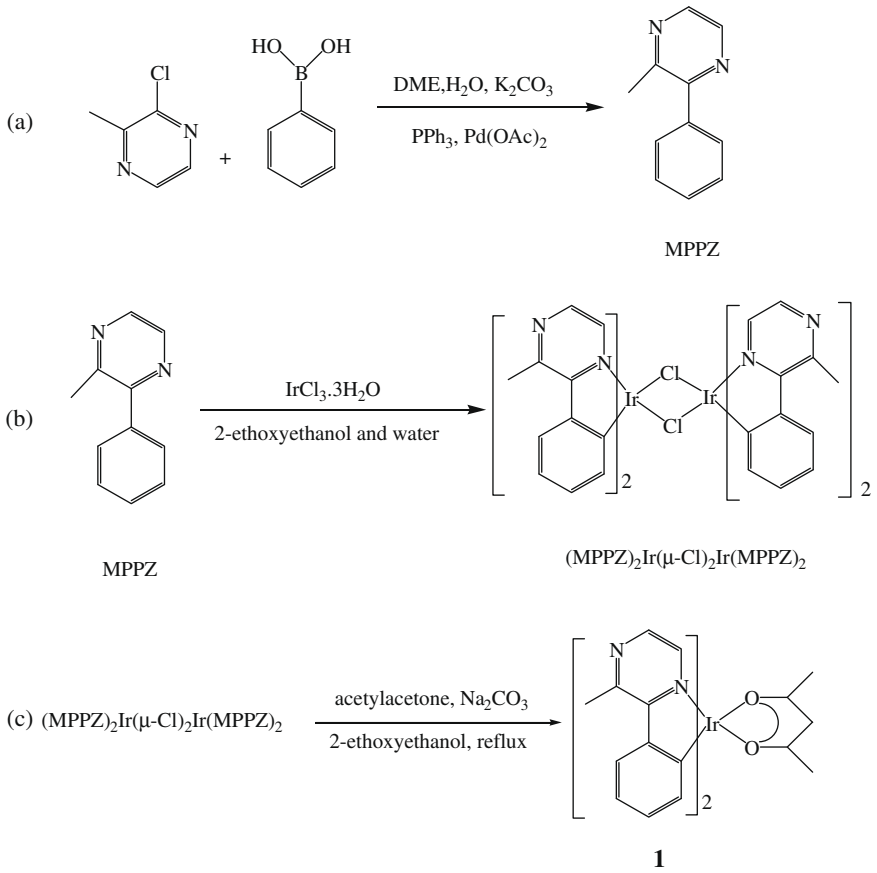

Scheme 1.

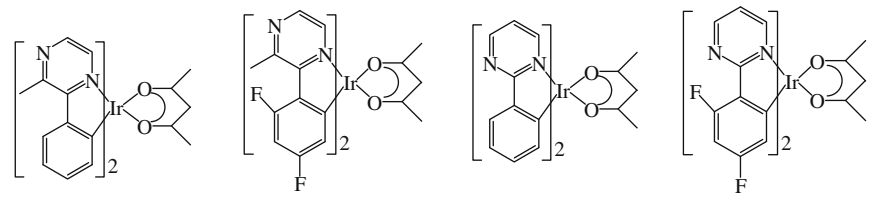

Chart 1.

1-Position nitrogen atom in **4-PPM** and **4-DFPPM** may react with Ir(III) resulting in many by-products (Fig. 1).

3.2. Photophysical data

The absorption and emission data of the complexes are summarized in Table 1. Fig. 2 shows the UV–Vis absorption and photoluminescence (PL) spectra of the complexes in dichloromethane at room temperature. All the complexes exhibit bands in the UV and in the visible region similar to those found for iridium phenylpyridine-type complexes. The bands below 350 nm are assigned to the spin-allowed $^1\pi$–π^* transition of diazine ligands, in the visible region weaker bands can be assigned to singlet and triplet MLCT transitions and $^3(\pi$–$\pi^*)$ transitions.

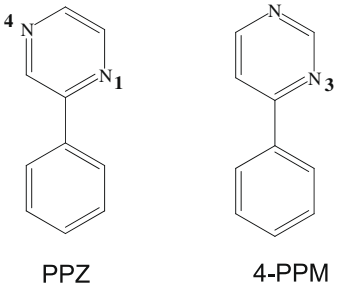

Fig. 1. The molecular structures of **PPZ** and **4-PPM**.

Table 1
Photophysical and electrochemical data for (**da**)$_2$Ir(acac).

(**da**)$_2$Ir(acac)	λ_{abs} (nm)	λ_{em}(fwhm) (nm)
(**MPPZ**)$_2$Ir (acac) (**1**)	258, 322, 410, 496	575(61)
(**DFMPPZ**)$_2$Ir(acac) (**2**)	258, 327, 410, 468	546(63)
(**PPM**)$_2$Ir(acac) (**3**)	261, 341, 406, 460	527(55)
(**DFPPM**)$_2$Ir(acac) (**4**)	256, 330, 396, 463	496(62)

fwhm, full width at half-maximum.

The low-energy MLCT band in complex **3** (460 nm) is significantly blue-shifted compared to that of complex **1** (496 nm) (Fig. 2). The iridium pyrazine complex **1** emits yellow light with a maximum peak at 575 nm, whereas the iridium pyrimidine complex **3** emits green light with a maximum peak at 527 nm (Fig. 2) that is in good consistent with their absorption spectra. The small Stokes shift between emission signal and the lowest energy absorption band in the iridium complexes, in combination with a structureless spectral feature, suggest that the phosphorescence originate primarily from the ^{3}MLCT state, together perhaps with a lesser contribution from the $^3\pi$–π^* excited states [3]. Similarly, compared with iridium pyrazine complex **2**, iridium pyrimidine complex **4** also shows a 50 nm blue-shift of the emission band. The results imply that the orientation of π conjugation would exert a large effect on the photophysical properties of the phosphorescent complexes. Replacing the phenyl fragment with a 2,4-difluorophenyl substituent in the cyclometalating ligand blue-shifted the emission wavelengths of the complexes from 575 and 527 nm to 546 and 496 nm, respectively (Table 1), by lowering the HOMO energy level of the cyclometalated ligand using two electronegative F atoms [3]. DFT calculations indicate that the highest occupied molecular orbital (HOMO) is mainly contributed from dπ states of the iridium atom and the relatively electron rich

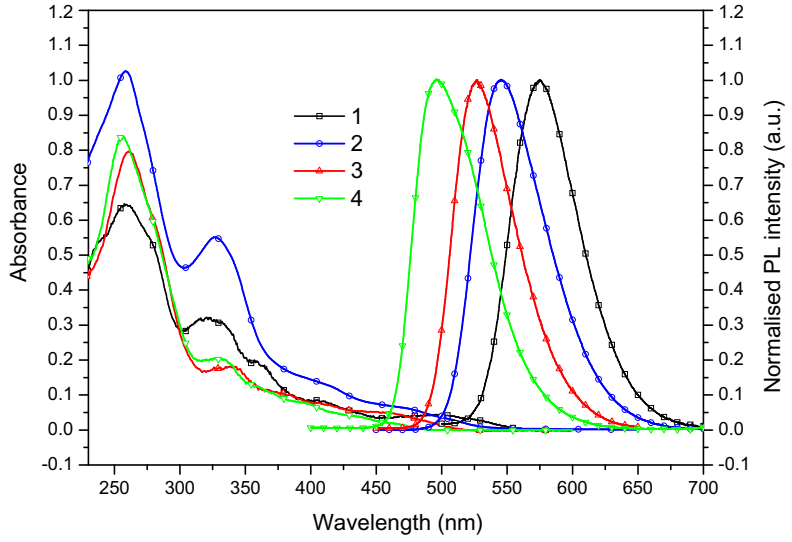

Fig. 2. UV–Vis absorption and PL spectra of (**da**)$_2$Ir (acac) in CH_2Cl_2.

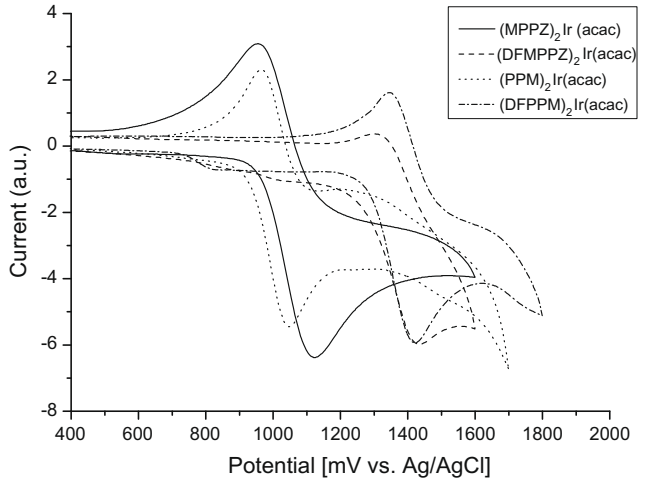

Fig. 3. Cyclic voltammograms of **1**, **2**, **3** and **4** in 0.1 M tetrabutylammonium hexafluorophosphate (TBAP) at a scan rate of 50 mV s^{-1}.

phenyl group of the cyclometalated ligand, whereas the lowest unoccupied molecular orbital (LUMO) is predominantly located at the N-heterocyclic part of the cyclometalated ligand [3,23]. When electron withdrawing groups were incorporated onto the phenyl ring, it will decrease the HOMO energy and thereby increase the HOMO–LUMO energy gap [24].

3.3. Electrochemical properties

Cyclic voltammetry (CV) was employed to investigate the electrochemical behavior of the complexes (**da**)$_2$Ir(acac). The highest occupied molecular orbital (HOMO) and lowest unoccupied molecular orbital (LUMO) energy levels of the materials were estimated according to the electrochemical performance and the UV–Vis absorption spectra. As shown in Fig. 3, the potentials for oxidation were observed to be 1.04, 1.37, 1.00 and 1.38 V, respectively. The oxidation potential, measured relative to a ferrocenium/ferrocene reference (Fc+/Fc), are listed in Table 2. The HOMO energy values for these iridium complexes were calculated based on the value of −4.8 eV for Fc with respect to zero vacuum level [25–27]. The electrochemical data and energy levels of the complexes are summarized in Table 2. The oxidation of the two fluorinated complexes occurred at significant more positive potentials (1.37 and 1.38 V) than the unfluorinated complex **1** (1.04 and 1.00 V). These values are similar to the reported bis-cyclometalated iridium complexes [3,28,29].

The HOMO–LUMO level of these Ir (III) complexes are also affected by the diazine group. This was revealed by the fact that substitution of the **MPPZ** ligand by the **PPM** ligand markedly raised the LUMO energy from −3.13 eV of **1** to −2.93 eV of **3**, while replacement of the **DFMPPZ** ligand with **DFPPM** led to a shift from −3.39 eV for **2** to −3.12 eV for **4**. It should be noted that minor changes at the HOMO were also observed (−5.31 eV for **1** and −5.27 eV for **3**; −5.64 eV for **2** and −5.65 eV for **4**; respectively). As a result, the pyrimidine complexes have a larger increase for the LUMO than the HOMO orbital, resulting in a widening of the HOMO–LUMO gap in comparison with the pyrazine complexes.

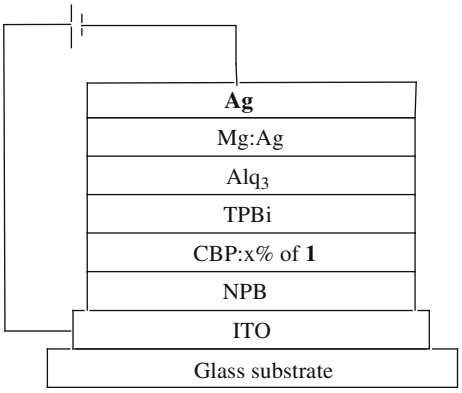

Device **A**: ITO/NPB(40 nm)/Ir:CBP(10%, 30 nm)/AlQ(50 nm)/Mg:Ag(150 nm, 10:1)/Ag(10 nm). Devices **B**–**D**: ITO/NPB(40 nm)/Ir:CBP(*x*%, 30 nm)/TPBi(15 nm)/AlQ(50 nm)//Mg:Ag(150 nm, 10:1)/Ag(10 nm) (*x* = 7.8, B; *x* = 10, C; *x* = 18, D).

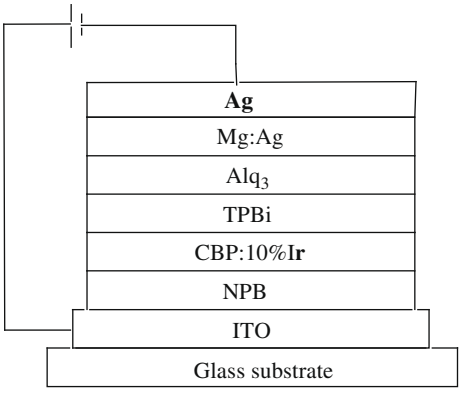

Device **E**: ITO/NPB(40 nm)/CBP:(**PPM**)$_2$Ir(acac)(10%, 30 nm)/TPBi(15 nm)/Alq$_3$(50 nm)//Mg:Ag(150 nm, 10:1)/Ag(10 nm). Device **F**: ITO/NPB(40 nm)/CBP:(PPY)$_2$Ir(acac) (10%, 30 nm)/TPBi (15 nm)/AlQ(50 nm)//Mg:Ag(150 nm, 10:1)/Ag(10 nm).

3.4. Electrophosphorescent properties

To illustrate the EL properties of the new Ir(III) complexes, multilayer OLED devices using complexes **1** and **3** as dopants in the

Table 2
Electrochemical potentials and energy levels of the iridium complexes.

Iridium complex	E^{ox} vs. Ag/AgCl (V)	E^{ox} vs. Fc (V)	E_g[a] (eV)	HOMO[b] (eV)	LUMO[c] (eV)
1	1.04	0.51	2.18	−5.31	−3.13
2	1.37	0.84	2.25	−5.64	−3.39
3	1.00	0.47	2.34	−5.27	−2.93
4	1.38	0.85	2.53	−5.65	−3.12

[a] Bandgap estimated from the UV–Vis absorption spectra.
[b] Calculated from the oxidation potentials.
[c] Deduced from the HOMO and E_g.

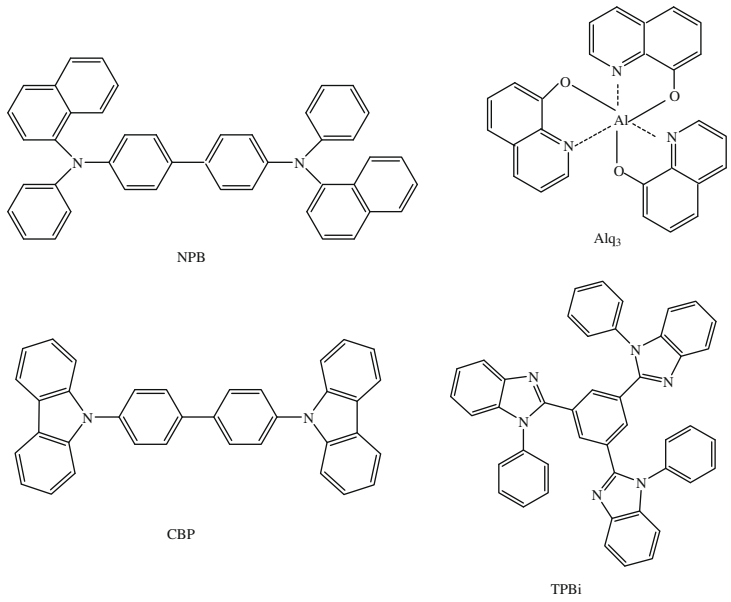

Fig. 4. The general structure for devices **A–F** and the molecular structures of the compounds used in these devices.

active emitting layer have been fabricated. Fig. 4 shows the general structure for device **A–F** and the molecular structures of the compounds used in the device. We have used CBP as the high triplet energy host for the iridium complexes because of its proven excellency as the host for iridium complexes and theoretical confirmation of favorable triplet energy [30]. Key characteristics of these devices are list in Table 3.

In devices **B–D**, TPBi was used as the electron-transporting/hole-blocking material and the CBP layer was doped with 7.8%, 10.0%, and 18.0% of **1,** respectively. All of these devices emitted orange-yellow light with an emission maximum at 580 nm. There are no characteristic emission peaks from CBP or Alq_3 even at high current density, indicating an effective energy transfer from the host exciton to the dopant. Meanwhile, there is no exciton decay in the Alq_3 layer due to the hole-blocking action of the TPBi layer. Correspondingly, the emission from Alq_3 was observed in the EL spectrum of device **A** without TPBi indicating that device **A** has excitons combined in the Alq_3 layer due to no effective hole-blocking action in the absence of TPBi (Fig. 5). In addition, device **A** shows a relative lower device efficiencies (Table 3), indicating TPBi has key role in the balance of electron and hole transport, giving highly efficient charge capture inside the device.

The EL spectrum of device **B** does not change significantly with variation of the applied voltage as show in Fig. 5. But compared with its PL spectrum peaking at 575 nm, the EL spectra of the device posed a major peak locating at 580 nm with a weak shoulder at 620 nm (Fig. 6). A similar phenomena was seen on $(tbt)_2Ir(acac)$ and $(tpbi)_2Ir(acac)$ reported by Wei et al. [31]. These phenomena may be assigned to the complex interactions among the CBP and iridium phosphors under the electric field, which cause the characteristic of $^3\pi$–π^* increases in EL excitation process compared to PL excitation process [31].

Comparison of the performances of devices **B–D** indicates that device **B**, with 7.8% of **1** shows the highest device efficiencies (Table 3). A turn-on voltage of 4.1 V, with a maximum brightness of 11565 cd/m^2 at 19.8 V, external quantum efficiency of 13.2% at 0.392 mA/cm^2, current efficiency of 37.3 cd/A at 0.392 mA/cm^2,

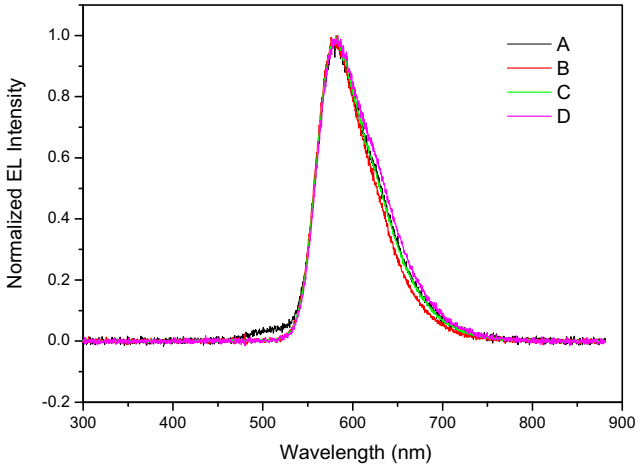

Fig. 5. The EL spectra of devices **A–D** with **1** as phosphor.

Table 3
Performance characteristics for OLEDs based on iridium complexes **1** and **3**.

Device	λ_{max} (nm)	V_{on} (V)	L_{max} (cd/m^2)	$\eta_{ext,max}$ (%)	η_{max} (lm/W)	η_{lmax} (cd/A)	100 cd/m^2		
							η_{ext} (%)	η (lm/W)	η_l (cd/A)
A	580	4.1	69548 (17.8)	5.4	5.4	14.6	4.0	5.1	11.0
B	580	4.1	111565 (19.8)	13.2	20.3	37.3	13.1	16.0	36.9
C	580	4.1	105774 (21.3)	12.4	14.7	33.8	11.6	13.2	31.6
D	580	3.7	96675 (17.8)	10.3	18.5	27.1	10.3	13.9	27.1
E	527	3.2	120450 (15.0 V)	13.9	48.6	58.2	12.9	35.5	53.7
F	522	3.1	153991 (18.5 V)	14.4	44.4	56.0	14.2	31.5	55.2

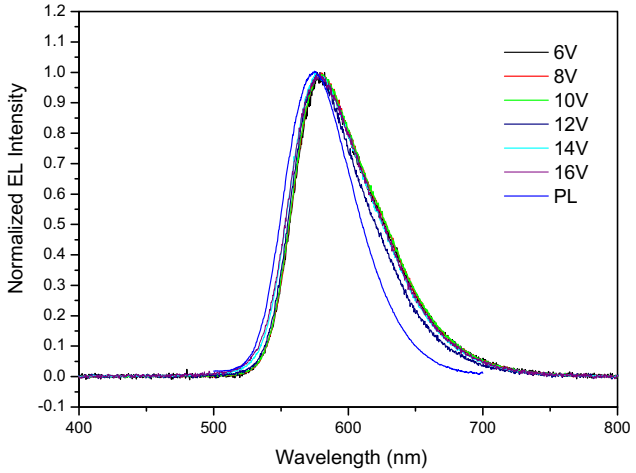

Fig. 6. The PL spectra of **1** and the electroluminescence spectra of device **B** at different voltages.

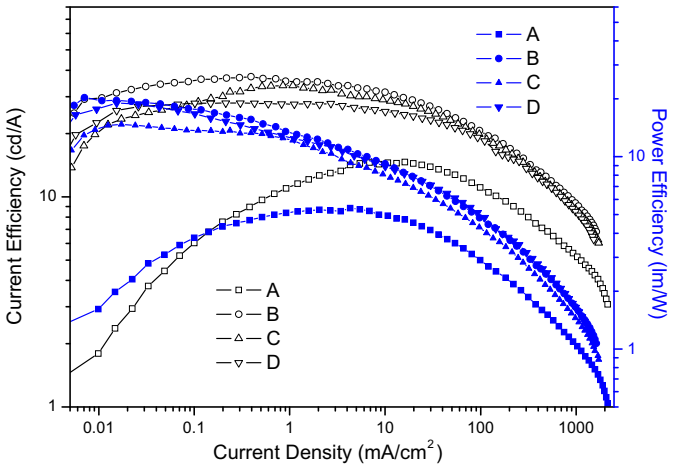

Fig. 8. The current efficiency–current– power efficiency characteristics of devices **A–D**.

and power efficiency of 20.3 lm/W at 0.00708 mA/cm^2, were achieved (Figs. 7–9). Furthermore, the efficiency of this device remained as high as external quantum efficiency of 7.4%, brightness of 21416 cd/m^2, current efficiency, 21 cd/A, power efficiency of 4.7 lm/W under driven current density of 100 mA/cm^2. The device showed a gradual decrease in η_{ext} with increasing current density, which is attributed to increasing triplet–triplet annihilation of the phosphor-bound excitons and field-induced quenching effects [6].

The performance of device **B** is comparable with those of $(fbi)_2Ir(acac)$ (brightness, 21105 cd/m^2; external quantum efficiency, 7.3%; current efficiency, 21 cd/A; power efficiency, 4.7 lm/W at a current density of 100 mA/cm^2) reported by Lin and co-workers [32] and favorably with those of $(bt)_2Ir(acac)$(brightness, 2500 cd/m^2 at a current density of 10 mA/cm^2; external quantum efficiency, 5.5% at a current density of 100 mA/cm^2) reported by Thompson and co-workers [6].

The performance of device **C** and device **D** at 10 wt% and 18% concentration, respectively, are also very remarkable (Figs. 7–9). Device **C** with turn-on voltage of 4.1 V has its highest brightness of 105774 cd/m^2 at 21.3 V, a maximum external quantum efficiency of 12.4%, a highest power efficiency of 14.7 lm/W and a highest current efficiency of 33.8 cd/A. Device **D** has lowest turn-on voltage of 3.7 V of the three devices, and its highest brightness of 96675 cd/m^2 at 17.8 V, a maximum external quantum efficiency

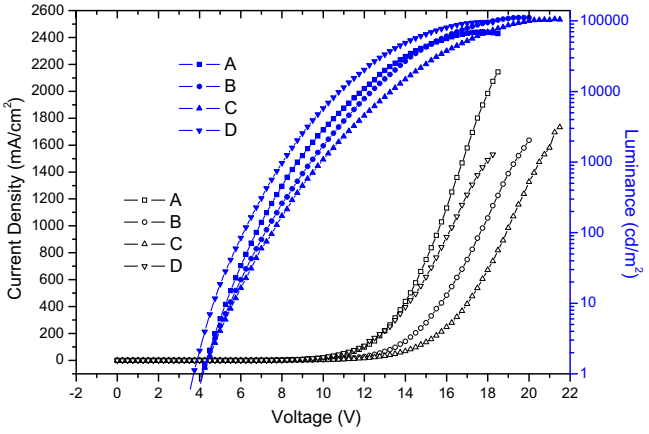

Fig. 7. The current–voltage– luminance characteristics of devices **A–D**.

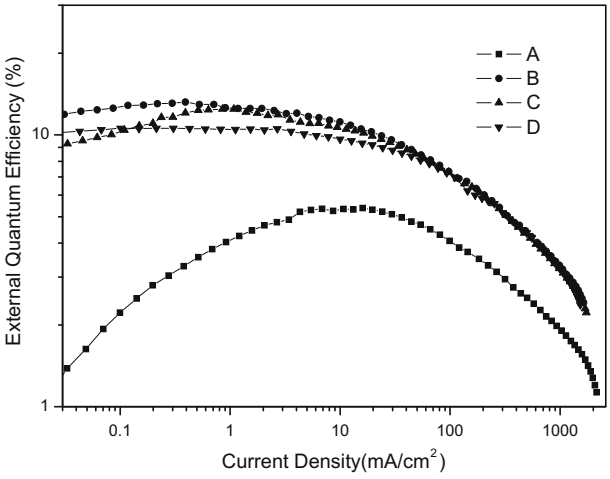

Fig. 9. The external quantum efficiency–current characteristics of devices **A–D**.

of 10.3%, a highest power efficiency of 18.5 lm/W and a highest current efficiency of 27.1 cd/A were achieved.

We have also fabricated two electroluminescent (EL) devices using **3** (device **E**) and $(PPY)_2Ir(acac)$ (device **F**) as dopants in the emitting layers. To compare the relative electroluminescent properties, the device structure and the thickness of the layers have been kept constant. Device **F** emits green light with an emission maximum at 522 nm, whereas replacement of one CH group at the pyridyl fragment by a nitrogen atom of the pyrimidine ligand in complex **3** makes the emission redshift. The performances of green emitting device **E** appear to be very promising, and its performance parameters are comparable with those of device **F**.

4. Conclusion

In summary, we got succeeded in preparation of four phosphorescent iridium (III) diazine complexes emitting yellow or green colors. The results suggest that steric influence of substituent group or symmetry of the ligand play a very important role in the cyclometalated procedure. Secondly, the iridium pyrimidine complexes show a significantly blue-shift of the emission band, compared with iridium pyrazine complexes. The iridium pyrazine complex **1** emits yellow light with a maximum peak at 575 nm, whereas the iridium pyrimidine complex **3** emits green light with

a maximum peak at 527 nm. Finally, very highly efficient OLEDs using the complexes **1** and **3** as the phosphorescent dopants have been demonstrated.

Acknowledgements

The works were supported by the National Nature Science Foundation of China (No. 20474003 and No. 90401028) and 973 Program, PR China (2002CB613405).

References

[1] X. Gong, M.R. Robinson, J.C. Ostrowski, D. Moses, G.C. Bazan, A.J. Heeger, Adv. Mater. 14 (2002) 581.
[2] C. Adachi, M.A. Baldo, M.E. Thompson, S.R. Forrest, J. Appl. Phys. 90 (2001) 5048.
[3] F.M. Hwang, H.Y. Chen, P.S. Chen, C.S. Liu, Y.C. Chi, C.F. Shu, F.L. Wu, P.T. Chou, S.M. Peng, G.H. Lee, Inorg. Chem. 44 (2005) 1344.
[4] P. Coppo, E.A. Plummer, L.D. Cola, Chem. Commun. (2004) 1774.
[5] A. Tsuboyama, H. Iwawaki, M. Furugori, T. Mukaide, J. Kamatani, S. Igawa, T. Moriyama, S. Miura, T. Takiguchi, S. Okada, M. Hoshino, K. Ueno, J. Am. Chem. Soc. 125 (2003) 12971.
[6] S. Lamansky, P. Djarovich, D. Murphy, F.A. Razzaq, R. Kwong, I. Tsyba, M. Bortz, B. Mui, R. Bau, M.E. Thompson, J. Am. Chem. Soc. 123 (2001) 4304.
[7] S. Lamansky, P. Djarovich, D. Murphy, F.A. Razzaq, R. Kwong, I. Tsyba, M. Bortz, B. Mui, R. Bau, M.E. Thompson, Inorg. Chem. 40 (2001) 1704.
[8] Y. You, S.Y. Park, J. Am. Chem. Soc. 127 (2005) 12438.
[9] M.K. Nazeeruddin, R. Humphry-Baker, D. Berner, S. Rivier, L. Zuppiroli, M. Graetzel, J. Am. Chem. Soc. 125 (2003) 8790.
[10] J. Li, P.I. Djurovich, B.D. Alleyne, M. Yousufuddin, N.N. Ho, J.C. Thomas, J.C. Peters, R. Bau, M.E. Thompson, Inorg. Chem. 44 (2005) 1713.
[11] A. Tsuboyama, H. Mizutani, S. Okada, T. Takiguchi, S. Miura, T. Moriyama, S. Igawa, J. Kamatani, M. Furugori, Eur. Pat. Appl. (2002) EP1191612.
[12] J.P. Duan, P.P. Sun, C.H. Cheng, Adv. Mater. 15 (2003) 224.
[13] Y.H. Song, S.J. Yeh, C.T. Chen, Y. Chi, C.S. Liu, J.K. Yu, Y.H. Hu, P.T. Chou, S.M. Peng, G.H. Lee, Adv. Funct. Mater. 14 (2004) 1221.
[14] Z.W. Liu, G. Min, Z.Q. Bian, D.B. Nie, Z.L. Gong, Z.B. Li, C.H. Huang, Adv. Funct. Mater. 16 (2006) 1441.
[15] G.L. Zhang, H.Q. Guo, Y.T. Chuai, D.C. Zou, Acta Chim. Sinica 63 (2005) 143.
[16] G.L. Zhang, Z.H. Liu, H.Q. Guo, Y.T. Chuai, C.G. Zhen, D.C. Zou, Chem. J. Chinese. Univ. 25 (2004) 397.
[17] G.L. Zhang, H.Q. Guo, Y.T. Chuai, D.C. Zou, Mater. Lett. 59 (2005) 3002.
[18] G.P. Ge, G.L. Zhang, H.Q. Guo, Y.T. Chuai, D.C. Zou, Inorg. Chim. Acta (2008), doi:10.1016/j.ica.2008.10.001.
[19] G.P. Ge, X.H. Yu, H.Q. Guo, F.Z. Wang, D.C. Zou, Synthetic Met. (2009), doi:10.1016/j.synthmet.2009.02.007.
[20] O. Lohse, P. Thevenin, E. Waldvogel, Synlett 1 (1999) 45.
[21] I. Helland, T. Lejon, Heterocycles 51 (1999) 611.
[22] M.B. Nonoyama, Chem. Soc. Jpn. 47 (1974) 767.
[23] Y.Y. Lyu, Y. Byun, O. Kwon, E. Han, W.S. Jeon, R.R. Das, K.J. Char, J. Phys. Chem. B 110 (2006) 10303.
[24] C.H. Yang, K.H. Fang, C.H. Chen, I.W. Sun, Chem. Commun. (2004) 2232.
[25] J. Pommerehne, H. Vestweber, W. Guss, R.F. Mahrt, H. Bässler, M. Porsch, J. Daub, Adv. Mater. 7 (1995) 551.
[26] M. Thelakkat, H.-W. Schmidt, Adv. Mater. 10 (1998) 219.
[27] X.W. Zhang, J. Gao, C.L. Yang, L.N. Zhu, Z.A. Li, K. Zhang, J.G. Qin, H. You, D.G. Ma, J. Organomet. Chem. 691 (2006) 4312.
[28] K. Dedeian, J.M. Shi, N. Shepherd, E. Forsythe, D.C. Morton, Inorg. Chem. 44 (2005) 4445.
[29] C.H. Yang, S.W. Li, Y. Chi, Inorg. Chem. 44 (2005) 7770.
[30] B.W. D'Andrade, M.A. Baldo, C. Adachi, J. Brooks, M.E. Thompson, S.R. Forrest, Appl. Phys. Lett. 79 (2001) 1045.
[31] X.Q. Wei, J.B. Peng, J.B. Cheng, M.G. Xie, Z.Y. Lu, C. Li, Y. Cao, Adv. Funct. Mater. 17 (2007) 3319.
[32] W.S. Huang, J.T. Lin, C.H. Chien, Y.T. Tao, S.S. Sun, Y.S. Wen, Chem. Mater. 16 (2004) 2480.